Ultrahigh efficiency EUV contact-hole printing with chromeless phase shift mask

Patrick Naulleau, Christopher N. Anderson, Weilun Chao, Kenneth A. Goldberg, Eric Gullikson, Farhad Salmassi, Antoine Wojdyla

Center for X-Ray Optics, Lawrence Berkeley National Laboratory, Berkeley, CA 94720

ABSTRACT

Contact-hole layer patterning is expected to be one of the first applications for EUV lithography. Conventional darkfield absorber masks, however, are extremely inefficient for these layers, placing even more burden on the already challenging source power demands. To address this concern, a checkerboard phase shift mask configuration has been proposed yielding theoretical throughput gains of 5x assuming a thin-mask modeling.

In this manuscript we describe the fabrication of such a mask and demonstrate its imaging performance using the SHARP EUV microscope and MET exposure tool at Lawrence Berkeley National Laboratory. For 25-nm dense features, the phase shift mask was shown to provide a throughput gain of 8x based on SHARP and 7x based on the Berkeley MET. The higher then predicted gain is expected to be due to the fact that the thin mask modeling used in the initial prediction misses shadowing effects.

Keywords: extreme ultraviolet, lithography, photomask, phase shift mask

1. INTRODUCTION

Contact-hole printing is expected to be one of the first high volume manufacturing applications of extreme ultraviolet (EUV) lithography [1,2]. Contact-hole printing, however, with conventional masks is highly inefficient placing even more burden on the already daunting challenge of EUV source power [3]. Figure 1 shows both dense 20 nm lines and spaces and contacts printed on the Berkeley MET tool [4,5] in an identical high resolution chemically amplified resist. While the line space features print at 31 mJ/cm^2, contact features of the same size require 78 mJ/cm^2 demonstrating the optical inefficiency of contact-hole patterning.

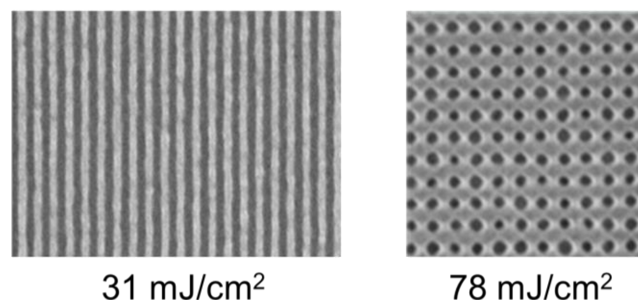

Fig. 1. Dense 20 nm lines and spaces and contacts printed in the Berkeley MET tool in an identical high resolution chemically amplified resist. While the line space features print at 31 mJ/cm^2, contact features of the same size require 78 mJ/cm^2.

This inefficiency in dose for contact-hole printing is not a result of resist limitations, but rather a mask effect. The typical modeled offset between dose to clear and dose to size for lines and spaces is approximately 2.2x, however, as shown in Fig. 2, this offset for contact holes printed using a conventional darkfield mask is 5x. The simulation shown in Fig. 2

Photomask Japan 2016: XXIII Symposium on Photomask and Next-Generation Lithography Mask Technology, edited by Nobuyuki Yoshioka, Proc. of SPIE Vol. 9984, 99840P
© 2016 SPIE · CCC code: 0277-786X/16/$18
· doi: 10.1117/12.2243321

Downloaded From: http://proceedings.spiedigitallibrary.org/ on 05/13/2016 Terms of Use: http://spiedigitallibrary.org/ss/TermsOfUse.aspx

assumes 20-nm dense contacts, a numerical aperture (NA) of 0.33, quadrupole illumination with optimized offset [6], and employs the thin mask model. The large loss in optical efficiency can be hypothesized to be the result of the mask absorbing 75% of the incoming light through a simple area argument. Under this assumption, significant efficiency gains could be achieved by using a chromeless phase shift mask [6].

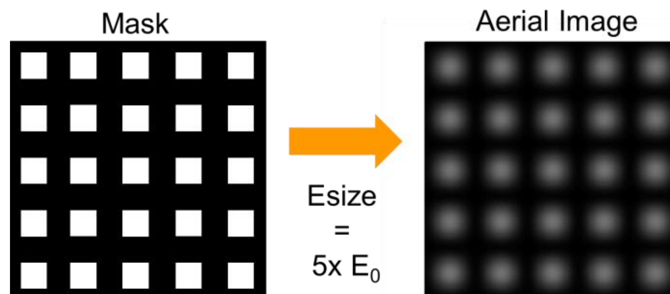

Fig. 2. Dense 20 nm contacts printing simulation assuming numerical aperture of 0.33, quadrupole illumination with optimized offset mJ/cm^2, and a thin mask model. A dose of 5x dose to clear is required to print the contacts at the desired size.

2. CHROMELESS PHASE SHIFT MASK EFFICIENCY

In a chromeless phase shift mask, there is no absorber on the mask and the binary features on the mask are simply comprised of equally reflective (or transmissive) regions but phase shifted relative to each other by 180º. In the simplest implementation, one would just keep the identical 2D morphology of the mask pattern, but replace the absorber regions with phase shifted regions (or its binary opposite which yields identical results). Figure 3 shows such a mask and its corresponding aerial image again for 20-nm dense contacts assuming 0.33 NA and a partial coherence [7] of 0.2.

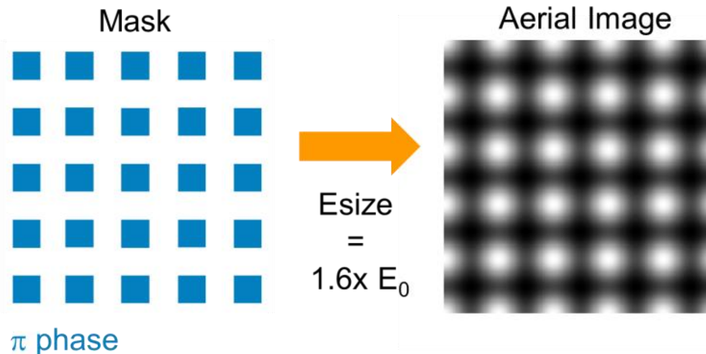

Fig. 3. Aerial image modeling results for a 20-nm dense contact pattern mask converted to chromeless phase shift demonstrating a significant improvement in optical efficiency compared to a darkfield absorber mask.

Figure 3 shows a significant improvement in efficiency compared to the darkfield mask, however, the aerial image also suggests a loss in contrast. This loss in contracts is quantified in Fig. 4 where we see the conventional mask to achieve an aerial image contrast of 90% while for the phase shift mask the aerial image contrast drops to 54%; which is arguably not really suitable for high quality patterning. The loss in contrast can be attributed to area imbalance between the 0º and 180º phase regions. For a contact-hole pattern, the only way to correct the phase imbalance is to employ a checkerboard design. Figure 5 shows such a design and the resulting aerial image again assuming an NA of 0.33 and a partial coherence of 0.2. Despite the mask pattern being checkerboard, the printed pattern remains a square grid. Also in this mode, the patterning exhibits pitch splitting which means that the mask patterning resolution requirements are relaxed by a factor of 2. Most importantly, we see a 5x gain in efficiency compared to the conventional absorber mask configuration. Also, we see an improvement in contrast relative to both the phase shift design from Fig. 3 as well as the conventional mask. A theoretical contrast of over 99% is observed (Fig. 6).

Downloaded From: http://proceedings.spiedigitallibrary.org/ on 05/13/2016 Terms of Use: http://spiedigitallibrary.org/ss/TermsOfUse.aspx

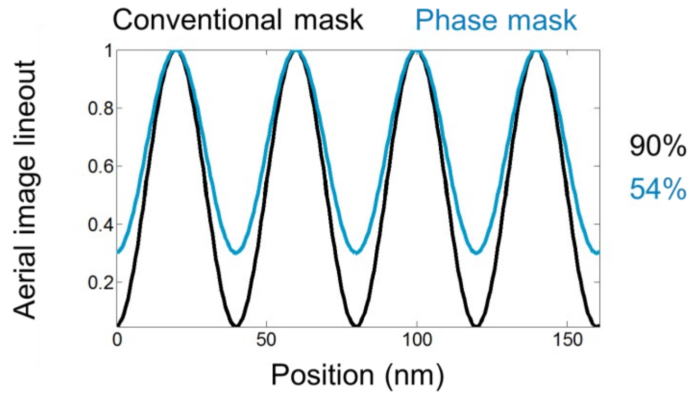

Fig. 4. Comparison of normalized aerial image lineouts for the two mask configurations considered above. The percent values on the right represent the aerial image contrast.

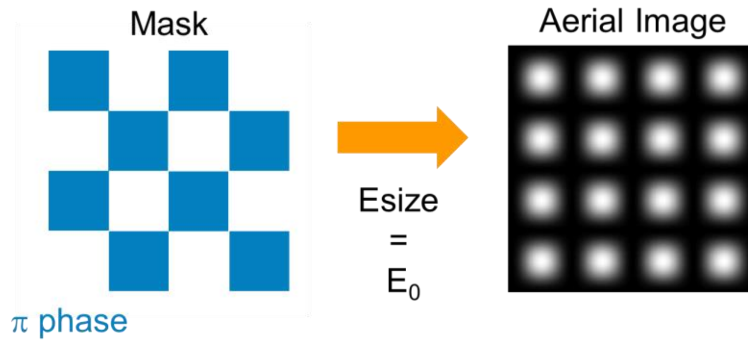

Fig. 5. Aerial image modeling results for a checkerboard phase mask designed to print a 20-nm dense contact pattern. A 5x improvement in efficiency compared to conventional absorber mask is observed. Modeling assumes NA = 0.33 and partial coherence = 0.2.

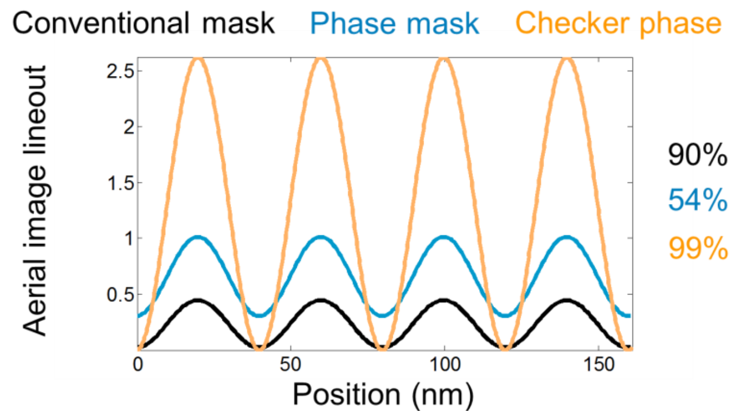

Fig. 6. Comparison of aerial image lineouts for the three mask configurations considered above. The percent values on the right represent the aerial image contrast.

Downloaded From: http://proceedings.spiedigitallibrary.org/ on 05/13/2016 Terms of Use: http://spiedigitallibrary.org/ss/TermsOfUse.aspx

3. FABRICATION

To test the real world performance of the checkerboard phase mask we used the etched multilayer phase shift mask method [8]. Figure 7 shows the fabrication process flow we followed. To facilitate the etch depth control requirements, we embedded a Cr etch stop within the multilayer film selecting the Cr thickness such that the upper portion of the multilayer stack remains phase locked to the lower portion. In addition to the embedded Cr etch stop, Cr is also used on top of the multilayer as a hard mask for the etch process. KRS e-beam resist is used to define the pattern transferred to the Cr hard mask. The resist is stripped and the multilayer etched using reactive ion etching stopping on the embedded Cr. The final step is to remove the residual Cr hard mask and etch stop.

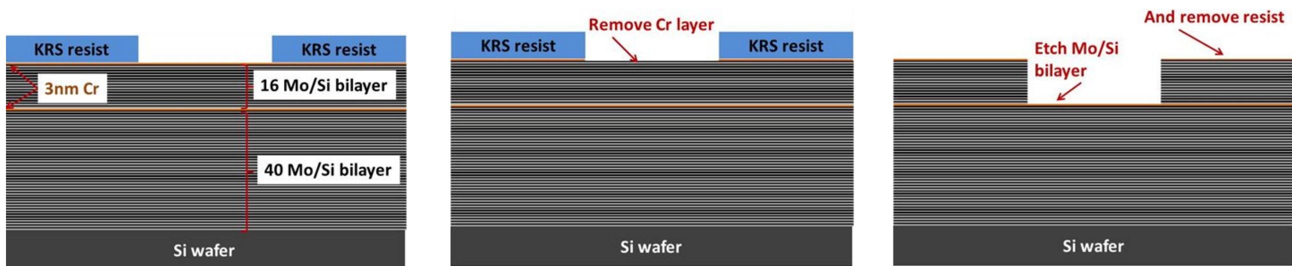

Fig. 7. Fabrication process flow for etched multilayer phase shift mask.

Figure 8 shows cross-section and top down scanning electron micrograph of the 25-nm coded features on the mask fabricated as described above. Assuming a 4x system and recalling the pitch splitting properties of the system, the square features on the mask itself are on the order of 200-nm wide. Corner rounding is observed in the top-down SEM, but modeling results (not shown) indicate the resulting imaging impact to be insignificant.

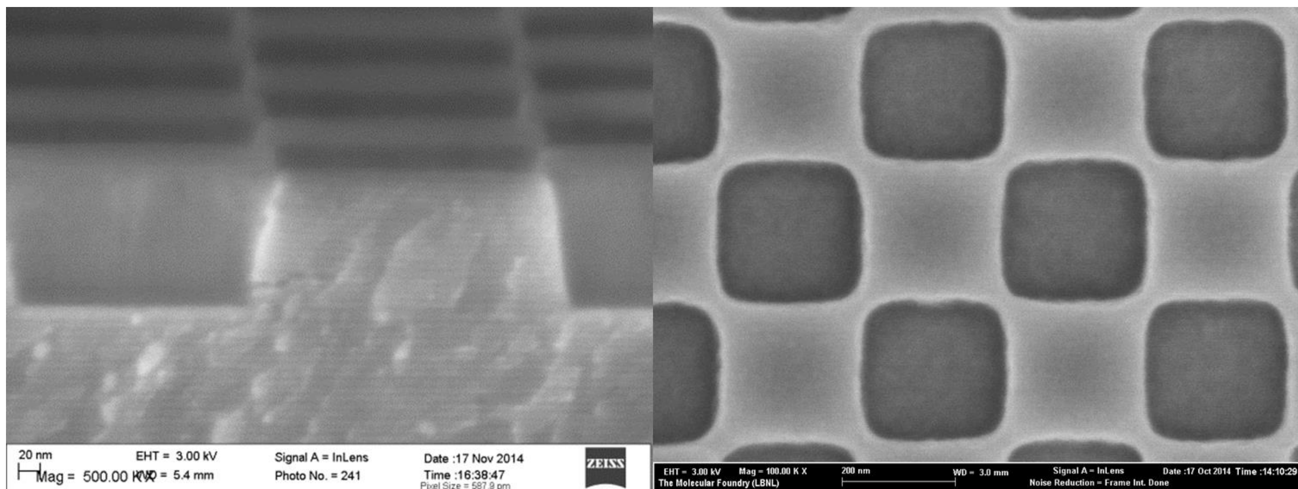

Fig. 8. Cross-section and top down scanning electron micrograph of the 25-nm coded features on the mask fabricated as described above..

Downloaded From: http://proceedings.spiedigitallibrary.org/ on 05/13/2016 Terms of Use: http://spiedigitallibrary.org/ss/TermsOfUse.aspx

4. AERIAL IMAGE CHARACTERIZATION

Initial imaging performance characterization of the checkerboard phase shift mask is performed using the SHARP EUV microscope at Berkeley [9] to mimic a 4x magnification exposure tool with wafer side numerical aperture of 0.33. Figure 9 shows a direct comparison of 25-nm half-pitch contact-hole imaging for the phase shift and conventional masks with identical dose conditions at the mask. The improved efficiency is readily evident through the observed difference in photon noise (pattern variability). The throughput gain is quantified by plotting the CD as a function of exposure level (Fig. 10) showing a throughput increase of 8x. Repeating the same measurements for 32-nm contacts, we find a throughput increase of 4.6x. The higher then predicted gain is expected to be due to the fact that the thin mask model used in the initial prediction neglects shadowing effects. Also evident from Fig. 10 is the 2x reduction in horizontal/vertical bias with the checker phase mask. For the 32-nm contacts, the reduction in bias is found to be 1.5x.

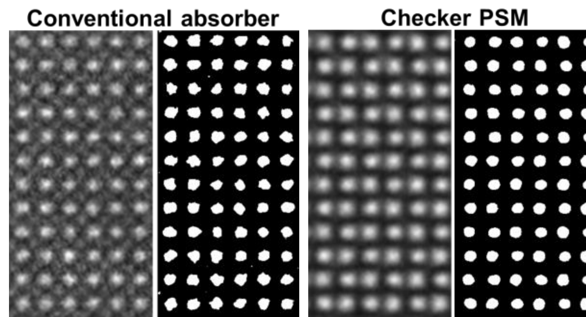

Fig. 9. Aerial imaging comparison in SHARP microscope of checkerboard PSM and conventional absorber masks for 25-nm dense contacts using identical exposure times.

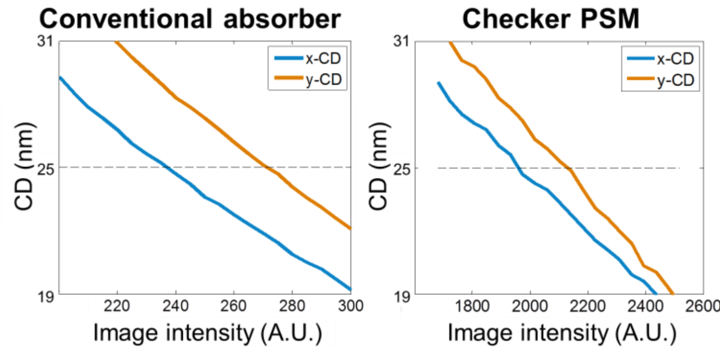

Fig. 10. Direct comparison of CD as a function of exposure level determined from SHARP aerial images for the checkerboard PSM and conventional absorber masks on 25-nm contacts.

5. LITHOGRAPHIC CHARACTERIZATION

Final characterization of the throughput gains provided by the checker phase mask compared to the conventional absorber mask was performed using the Berkeley MET exposure tool. We again consider 25-nm contacts at the wafer, but the MET being a 5x tool, the checker features on the mask are now 250-nm wide. For the print test we use a conventional high resolution chemically amplified EUV resist that readily achieves 16-nm line-space resolution. For both masks, an optimized quadrupole illumination setting was used. Figure 11 shows that the conventional absorber mask required a dose to size of 94 mJ/cm^2 whereas the checker phase mask achieved a dose of only 13 mJ/cm^2 (a throughput gain of approximately 7x). It is important to note that in reality the amount of dose getting to the wafer in both cases is actually the same as must be the case given that the resist is identical. What is different in the two cases is the dose delivered to the mask with the checker phase mask being much more efficient in terms of transferring that dose to the wafer. This is a crucial point because it means that the increase in speed does not come with an increase in shot noise as would be the case if the speed gains had been achieved by increasing the sensitivity of the resist.

Downloaded From: http://proceedings.spiedigitallibrary.org/ on 05/13/2016 Terms of Use: http://spiedigitallibrary.org/ss/TermsOfUse.aspx

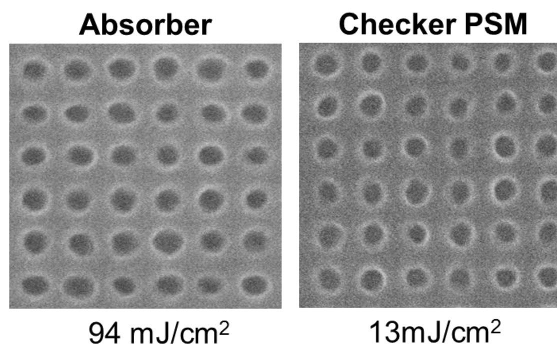

Fig. 11. Direct lithographic patterning comparison of conventional and checker phase masks in the Berkeley MET tool. Patterning of 25-nm contacts shows checker phase mask to provide a 7x efficiency gain relative to conventional absorber mask.

6. SUMMARY

Contact-hole patterning with a checkerboard chromeless EUV phase shift mask has been demonstrated. For 25-nm dense features, the phase shift mask was shown to provide a throughput gain of 8x based on aerial image characterization using the Berkeley SHARP microscope and 7x based on lithographic patterning in a chemically amplified resist using the Berkeley MET. Another benefit of the checkerboard phase mask is that is provides pitch splitting capabilities relaxing the mask patterning requirements.

The imaging, patterning, and modeling work was funded by Intel and Samsung. The authors also acknowledge Applied Materials, Inpria, JSR, and TSMC. We thank SEMATECH for early support in the fabrication of the phase shift mask. The imaging and patterning work was conducted by the Center for X-Ray Optics at the Lawrence Berkeley National Laboratory Advanced Light Source synchrotron radiation facility. The Advanced Light Source is supported by the Director, Office of Science, Office of Basic Energy Sciences, of the U.S. Department of Energy under Contract No. DE-AC02-05CH11231.

REFERENCES

1. Alberto Pirati, et al., "EUV lithography performance for manufacturing: status and outlook," Proc. SPIE **9776**, 97760A (2016).
2. Britt Turkot, Steven L. Carson, Anna Lio, Ted Liang, Mark Phillips, Brian McCool, Eric Stenehjem, Tim Crimmins, Guojing Zhang, Sam Sivakumar, "EUV progress toward HVM readiness," Proc. SPIE **9776**, 977602 (2016).
3. A. Schafgans, et al., "Performance optimization of MOPA pre-pulse LPP light source," Proc. SPIE **9422**, 94220B (2015).
4. P. Naulleau, et al., "Status of EUV microexposure capabilities at the ALS using the 0.3-NA MET optic," Proc. SPIE **5374**, 881-891 (2004).
5. C. Anderson, et al., "The SEMATECH Berkeley MET: demonstration of 15-nm half-pitch in chemically amplified EUV resist and sensitivity of EUV resists at 6.x-nm," Proc. SPIE **8322**, 832212 (2012).
6. H. J. Levinson, *Principle of lithography, second edition*, Chapter 8, 273, SPIE Press, Bellingham WA (2005)
7. H. J. Levinson, *Principle of lithography, second edition*, Chapter 5, 139, SPIE Press, Bellingham WA (2005)
8. Sang-In Han, Eric Weisbrod, Qianghua Xie, Pawitter J. S. Mangat, Scott D. Hector, William J. Dauksher, "Design and method of fabricating phase-shift masks for extreme-ultraviolet lithography by partial etching into the EUV multilayer mirror," Proc. SPIE **5037**, 314 (2003).
9. K. Goldberg, et al., "The SEMATECH high-NA actinic reticle review project (SHARP) EUV mask-imaging microscope," Proc. SPIE. **8880**, 88800T (2013)

Downloaded From: http://proceedings.spiedigitallibrary.org/ on 05/13/2016 Terms of Use: http://spiedigitallibrary.org/ss/TermsOfUse.aspx